

Climatology and classification of Spring Saharan cyclone tracks

A. Hannachi · A. Awad · K. Ammar

Received: 22 December 2009 / Accepted: 26 October 2010 / Published online: 10 November 2010
© Springer-Verlag 2010

Abstract Spring Saharan cyclones constitute a dominant feature of the not-well-explored Saharan region. In this manuscript, a climatological analysis and classification of Saharan cyclone tracks are presented using 6-hourly NCEP/NCAR sea level pressure (SLP) reanalyses over the Sahara (10°W–50°E, 20°N–50°N) for the Spring (March–April–May) season over the period 1958–2006. A simple tracking procedure based on following SLP minima is used to construct around 640 Spring Saharan cyclone tracks. Saharan cyclones are found to be short-lived compared to their extratropical counterparts with an e-folding time of about 3 days. The lee side of the west Atlas mountain is found to be the main cyclogenetic region for Spring Saharan cyclones. Central Iraq is identified as the main cyclolytic area. A subjective procedure is used next to classify the cyclone tracks where six clusters are identified. Among these clusters the Western Atlas–Asia Minor is the largest and most stretched, whereas Algerian Sahara–Asia Minor is composed of the most long-lived tracks. Upper level flow associated with the tracks has also been examined and the role of large scale baroclinicity in the growth of Saharan cyclones is discussed.

Keywords Cyclone tracks · Saharan region · Cyclone lifecycles · Track clusters

1 Introduction

The climate of the Saharan region plays an important role in the dynamics of the global climate system through, e.g. its radiative properties and its mineral dust source. For instance, it is well known that the North African continent, and more precisely the Saharan desert, represent a dominant global source of aeolian and mineral dust (Prospero et al. 2002; Washington et al. 2003) causing large dust plumes that are transported to the surrounding regions and beyond (see, e.g. Guerzoni and Chester 1996). For example, during the Saharan Mineral Dust Experiment (SAMUM-1) over southern Morocco (Heintzenberg 2009) long-range transport event of Saharan dust to southern Europe has been observed (Müller et al. 2009). There is a general tendency to believe that high pressure systems always prevail over the Sahara. Contrary to this general perception, cyclones are generated all year round in the Sahara. Saharan cyclogenesis, with its large intraseasonal and interannual variability, is another important feature of Saharan climate because of its role in transporting energy poleward and possibly initiating dust storms. The major stirring mechanism of Saharan and also Mediterranean cyclogenesis are thought to be associated either with large-scale circulation regimes, such as the effect of the North Atlantic troughs over the western African coast (Barry and Chorley 1992; Thorncroft and Flocas 1997) or local effects, such as low-level baroclinicity induced by sea–land contrast or local orography such as the Atlas mountains. The study of Saharan cyclones and their tracks, however, has received little attention from climate scientists, see e.g.

A. Hannachi (✉)
Department of Meteorology, Reading University,
PO Box 243, Reading RG6 6BB, UK
e-mail: A.Hannachi@reading.ac.uk

A. Awad
Department of Meteorology, King Abdulaziz University,
Jeddah, Saudi Arabia

K. Ammar
Department of Research, Meteorological Authority,
Cairo, Egypt

Elfandy (1940); Tantawy (1969); Pedgley (1972) and Alpert and Ziv (1989), and therefore is not well explored compared to extratropical regions such as the North Atlantic.

It is known, for instance, that Saharan cyclones constitute one of the dominant features in the region during the spring time, and where the southern and south-eastern parts of the Atlas mountains become major cyclogenesis sources in spring season March–May (MAM) and early June. Spring season is chosen here because it is an active season in the Saharan region (Trigo et al. 1999) during which the desert reaches considerable heating. It is also a period of frequent storms and flash floods in Arabia when precipitation is at its peak. Many of these storms are caused by perturbations initiated in the Sahara. The remaining seasons are also important for water resources in Arabia but will be investigated in a separate study. The Middle East and the Arabian peninsula are among the regions that have been under water stress in recent decades.

As the Siberian High, which dominates Eurasia and the Middle East in the winter, starts to weaken towards late winter/early spring and collapses in May there is indication that pressure in the Middle East also starts to decrease (Panagiotopoulos 2005). This pressure decrease extends to the Saharan region and initiates Saharan cyclogenesis. Other factors, such as large scale interactions, also contribute to Saharan cyclogenesis. For example, the southward shift of the polar jet, strengthening the wobbling of the subtropical jet (Thorncroft and Flocas 1997) and the effects of local radiative processes play a non-negligible role in Saharan cyclone formation. During late spring/early summer the onset of the Asian Monsoon acts remotely, via its descending cell over the Mediterranean (Rodwell and Hoskins 1996) to inhibit cyclogenesis in the Middle East and the Sahara in late spring and summer months, partly explaining the dry conditions in those regions in the summer (Trigo et al. 1999). In addition to the previous setting up factors of Saharan cyclogenesis, it is also thought that lee cyclogenesis constitutes the main initiation mechanism, and plays an important role in the growth, development and variability of Saharan lows (Egger et al. 1995).

In this study we focus on cyclones generated in the Sahara. These cyclones affect various regions around the Mediterranean particularly the Middle East and the Arabian peninsula and constitute an important source of water there. Other places, e.g. the Indian Ocean, also affect the Arabian peninsula and will be addressed in a future study. In addition, given the importance of the Saharan region in the global heat budget and energy balance, an objective analysis of the climatology of cyclone behaviour for the region would be of great benefit for many areas of climate science including the study of the dynamics of the atmosphere in the subtropical margins, the relationship between

cyclones and air–sea fluxes, the physical parametrization in climate models, and the study of projections of future cyclone climatologies and their effects on the local weather, e.g. in a warmer climate (e.g., Ulbrich et al. 2009).

The earlier compilations of storm tracks were based on the visual identification of cyclones and their paths from synoptic charts (Petterssen 1956; Klein 1957; HMSO 1962; Hayden 1981; Radinovic 1987; Flocas 1988; and Agee 1991). The availability of both high density observed gridded data and reanalyses opened the way to a large number of studies applying manual, semi-automated and automated procedures to detect and track storms (Alpert et al. 1990; Blender et al. 1997; Trigo et al. 1999; Sickmoller et al. 2000; Gulev et al. 2001; Hodges et al. 2003; Hanson et al. 2004). The climatology of cyclone characteristics, e.g. cyclone track density and orientation, intensification rate, and cyclo-genetic/lytic areas, give detailed information on typical cyclone life cycles for different regions (Pinto et al. 2005).

A number of cyclone tracking methods exist in the literature. Raible et al. (2008) compared three cyclone detection and tracking schemes (Blender et al. 1997; Murray and Simmonds 1991; Wernli and Schwierz 2006) using a 30-year period (1961–1990) of the European Reanalysis (ERA40) 1,000 hPa geopotential height. They conclude that overall the different schemes show good correspondence with a rather small structural difference. Although many studies on cyclone tracks have been performed over various places on the globe, such as the North Atlantic and the Mediterranean, very few studies, however, have been performed on the Saharan region (Thorncroft and Flocas 1997; Horvath et al. 2006). Horvath et al. (2006), for example, have investigated the effect of atmospheric conditions on cyclone tracks. One of the most important results of Horvath et al. (2006) is that the different paths of cyclones in the Mediterranean region are associated with different atmospheric factors affecting the system. So cyclone track classification is an important step in the identification of the effect of the atmospheric circulation regimes.

Studies by Trigo et al. (1999) and Trigo (2006) focussed particularly on the Mediterranean region using a rather short period (18 years) of ERA40. In this study we attempt to fill in this gap by contributing to the literature of cyclone tracks by exploring track characteristics in the not-well-explored Saharan region using a much longer period (49 years) of the National Center for Environmental Prediction–National Center for Atmospheric Research (NCEP–NCAR) reanalyses (Kalney et al. 1996; Kistler et al. 2001). In this paper the focus is mainly on the statistics and clustering of Saharan cyclone tracks during the spring (MAM) season. The association between the

different tracks and the large scale teleconnection is under investigation and will be reported elsewhere. The data and methodology are presented in Sect. 2. Section 3 presents the application to cyclone tracks identification and explores climatological track features. Cyclone tracks clustering along with the synoptic feature of the tracks are presented in Sect. 4, and a summary and discussion are presented in the last section.

2 Data and methodology

The data used for this study consist of 6-hourly sea level pressure (SLP) for the period 1958–2006. The data come from the National Center for Environmental Prediction and the National Center for Atmospheric Research (NCEP/NCAR) Reanalyses (Kalnay et al. 1996, Kistler et al. 2001) and have a spatial resolution of $2.5^\circ \times 2.5^\circ$ in the latitude/longitude directions. The NCEP/NCAR Reanalyses are based on a spectral model, with a 3D-Var data assimilation scheme used throughout the whole reanalysed period. Impact studies of the effect of the assimilation of satellite data, that became available only since 1979 onwards, show that the Northern Hemisphere is not greatly affected by the use of satellite retrievals, in contrast to the Southern Hemisphere, where conventional observations are sparser (Kistler et al. 2001; Andrae et al. 2004). Our study domain, shown in Fig. 1, is 10°W – 50°E , 20°N – 50°N .

Although the results that we will discuss refer to MSLP we have also used temperature, vorticity and potential vorticity fields. The results indicate, however, that MSLP field is satisfactory and can be used on its own for cyclone tracking, given that this field is smoother than, e.g. vorticity or surface temperature, and is also less prone to high frequency noise. Other authors (Schinke 1993; WASA 1998;

Alexandersson et al. 2000; Gulev et al. 2001; Hoskins and Hodges 2002) have also used MSLP for cyclone tracking. Hoskins and Hodges (2002), for example, find that MSLP and vorticity produce qualitatively the same result for cyclone identification on the synoptic scale. At the same resolution, however, vorticity generally produces more systems because of its focusing on smaller scales. Moreover, Simmonds et al. (1999) indicate that inclusion of upper air data, in relation to cyclone tracking, does not significantly change tracks' characteristics.

Figure 2 shows the (6-hourly) spring climatology of SLP over the study area. Low pressure is seen over most of the subtropical North Africa, particularly over western Sahara and most of Arabia. The variance map of the daily spring SLP is shown in Fig. 3a. The map also shows high variance over the Sahara and Eastern Arabia. Because of the importance of high frequency variance for cyclonic activity, we also show in Fig. 3b the 2–6 days variance of filtered SLP obtained using a Lanczos filter (Duchon 1979). Note in particular the diffluent structure of contours upon entering the Mediterranean with a particular increase of variance over the Sahara with a peak in Southern Tunisia. Note also a similar trough line over Eastern Arabia.

The majority of Saharan cyclones traverse the Atlas mountain chain mostly from the west and sometimes from the northwest. Upon moving over the mountains the surface low pressure weakens, due to potential vorticity conservation, and may disappear over the mountain peaks. Upon leaving the mountain peaks low pressure systems are then generated in the lee of the Atlas mountains. Similar behaviour is also noted for the Adriatic region (Horvath et al. 2006), midlatitude cyclones crossing the Rockies (Chung et al. 1976; Bannon 1992; Hoskins and Hodges 2002), and tropical cyclones (Lin et al. 2005).

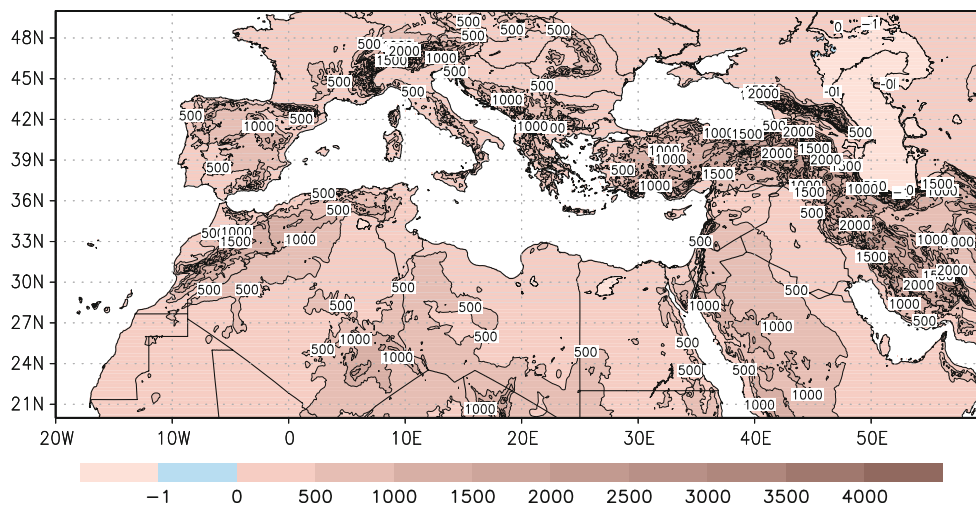


Fig. 1 Geographic map and surface elevation (m) of the study area. Contour interval 500 m

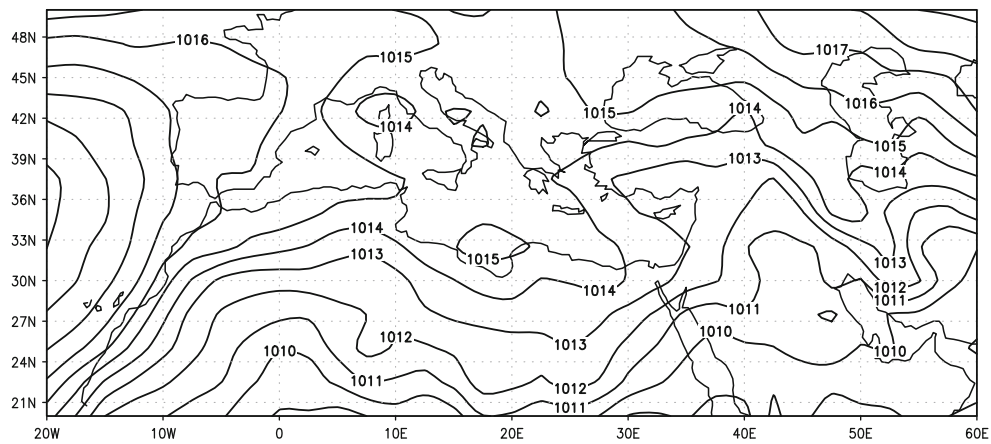


Fig. 2 Six-hourly SLP climatology over the study area during the spring season March–May (MAM) for the period 1958–2006. Contour interval 1 hPa

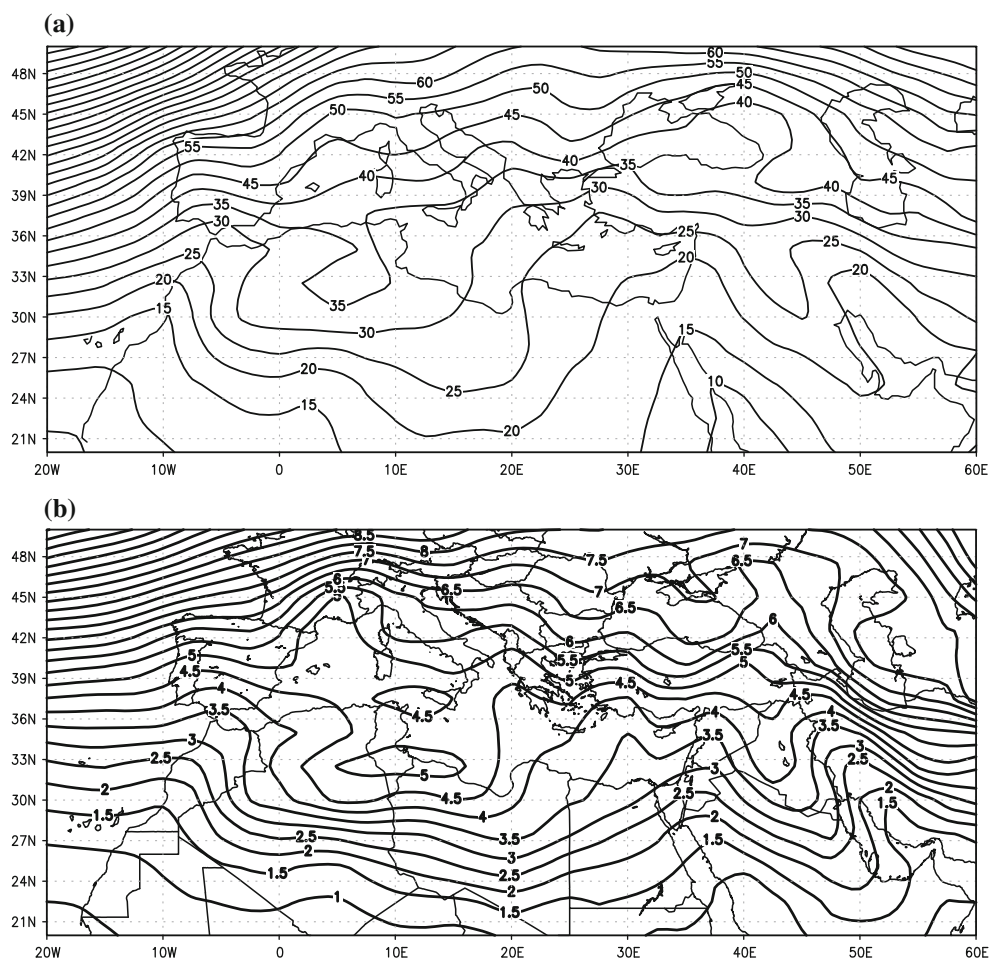


Fig. 3 Variance map spring (MAM) daily (*top*) and 2–6-day high pass filtered (*bottom*) SLP for the period 1958–2006. Contour interval 5 hPa² (*top*) and 0.5 hPa² (*bottom*)

Given that most Saharan cyclones are generated¹ in the lee of the Atlas chain (Fig. 1) we have chosen to restrict

¹ Or regenerated.

our search for cyclones that are generated within (10°W–25°E, 22°N–32°N) but the tracking is carried on way beyond this quadrant. The simple methodology developed here is composed of detection and tracking schemes. The

detection scheme is similar to that of Hanson et al. (2004) in that the SLP in the central (target) grid point is lower, by at least 0.8 hPa, than the surrounding eight grid points and is smaller than a threshold value of 1,008 hPa, in a similar manner to Hoskins and Hodges (2002) and Trigo et al. (2002). Note that the latter authors used 1,010 hPa as threshold. In addition, because Saharan cyclones are shallower than their midlatitude counterparts we require that the pressure difference between the target grid point and surrounding grid points is not larger than 3.8 hPa. This value is approximately twice the mean standard deviation of high frequency variance over the Sahara (Fig. 3).

After a cyclone centre is detected, within the initial search area, we then track it as far as 50E using a $60^\circ \times 30^\circ$ latitude–longitude box (10°W – 50°E , 22°N – 50°N). During the detection of the cyclone track the search routine is continuously updated from within the initial search area according to the following steps.

- After a cyclone centre is detected we track it for the next 12 h using a polygon containing 20 grid points surrounding the target grid point as shown in Fig. 4. During the search we go west and east, and north and south of the target grid point. To take into account the fact that some cyclones can shift north-westward, from time to time, we allow the search direction to go one step westward for each northward or southward step (Fig. 4). Trigo et al. (2002) define rather arbitrarily the search area to be 330 km in the zonal direction and 660 km in other directions. Whilst the non-isotropy of the search area may be a source of bias, we have also applied an isotropic search but the results have not changed.
- If, for a given day, there is more than one cyclone centre in the initial area we start the new track with the most eastern one and store the remaining centres in a potential track array, arranged in decreasing order of their longitudes. These centres will be used in the next time step as initial seeds for a new track search.
- If in the next two timesteps, that is for a duration of 12 h, no cyclone centre is detected, we consider the track has terminated. A new track search begins using initial grid points from the potential track array.

In any cyclone identification scheme core positions resulting from the procedure cannot be located between grid points when coarse grid input data are used. This difficulty has led some researchers to transform the data, e.g. by interpolation, to a finer grid prior to the application of the identification procedure (Alpert et al. 1990; Hodges 1995; Haak and Ulbrich 1996). Note that the main objective of interpolation is to allow the off-grid location to be found and also to allow a polar projection to be used for

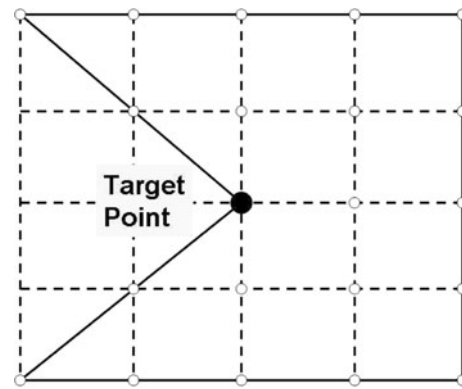


Fig. 4 Polygon search, containing 20 grid points (open circles) around the target grid point (filled circle), used for local cyclone tracking

identification particularly at higher latitudes. Interpolation between grid points is also used here to determine cyclone cores.

3 General characteristics of the Sahran cyclone tracks

3.1 Procedure validation

The procedure has been tested by comparing the obtained tracks with tracks obtained manually for the same dates. Six randomly chosen tracks have been selected and used for procedure validation. The (manually) identified tracks for these cases are followed step-by-step during the cyclones' life cycles. Figure 5 shows both the manually obtained tracks (dashed) and the automated ones (continuous). The agreement is extremely good in terms of both features of cyclone track paths and track time steps. The slight mismatch between the manual and automated tracks is due to the way the cyclone centre is specified. Whereas the visual tracking uses a cursor pointer on the map to specify the cyclone's centre, the automated routine finds the minimum value of the field at each time step. But the difference between these tracks (Fig. 5) can be virtually neglected.

The procedure is now applied to the full dataset from 1958 to 2006 during the spring time, i.e. March–April–May (MAM). A total of 643 tracks are identified. This set is smaller compared to sets from other studies based on the North Atlantic and European sectors. Saharan cyclones are expected to be less frequent than, e.g. their North Atlantic analogs. Also, comparing cyclone frequencies between ERA40 and NCEP/NCAR reanalyses, Raible et al. (2008) found that the latter reanalyses contain less cyclones than the former. The application to higher resolution reanalyses such as the European Centre for Medium Weather Forecast (ECMWF) Interim data and comparison with other existing

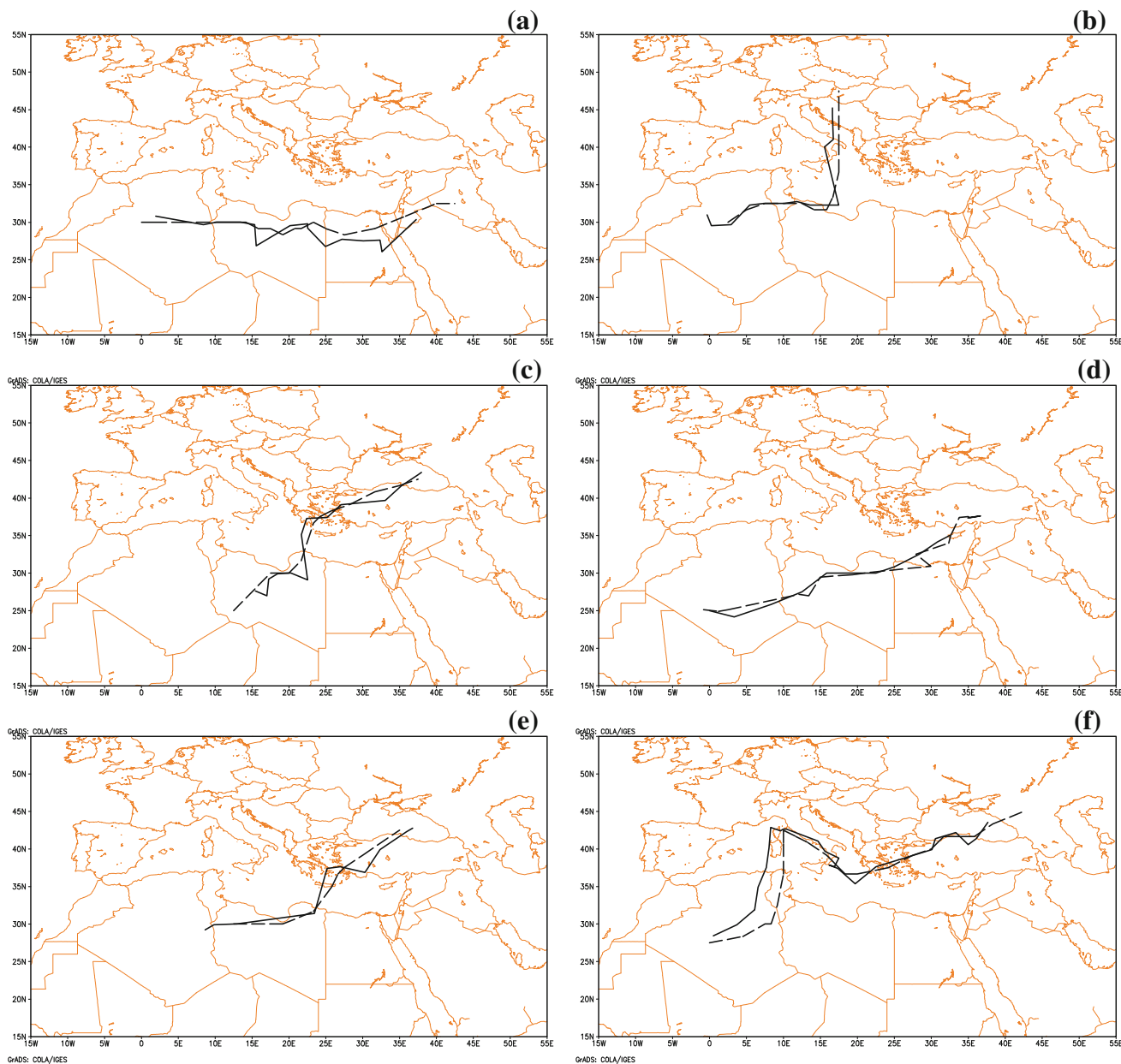


Fig. 5 Manually (*dashed*) and routinely (*continuous*) identified tracks

cyclone tracks will be addressed in a future study. Figure 6 shows the density of the obtained cyclones. The majority of tracks are initially zonally stretched with an increase of cyclones near the western Algerian border. Cyclones then deflect slightly south-eastward and increase in intensity near east Libya. Finally, the majority of tracks travel north-eastward with another increase of cyclogenesis over Turkey.

The identified tracks have different characteristics, length, orientation and longevity. To explore the characteristic features of these tracks we plot in Fig. 7 the number of Saharan cyclone tracks defined by their longevity in terms of the associated cyclones' lifecycles. The dark shading refers to all tracks and the light shading refers to

long tracks, defined as those tracks spanning (arbitrarily) more than 20° latitude or 10° longitude. When all tracks are used we get an approximate exponential decrease of the number of tracks with increasing lifespan, with an e-folding time of about 3 days, and the large majority of the tracks, around 90.4%, have longevity of 4 days or less.² The contribution from the 4-day lifespan in our case is around 9% compared to 2% in Hanson et al. (2004), due to the faster moving cyclones in the midlatitude, particularly

² A similar percentage of North Atlantic cyclones, with lifespan of 3 days or less, was found by Hanson et al. (2004) using both the ECMWF and NCEP/NCAR MSLP.

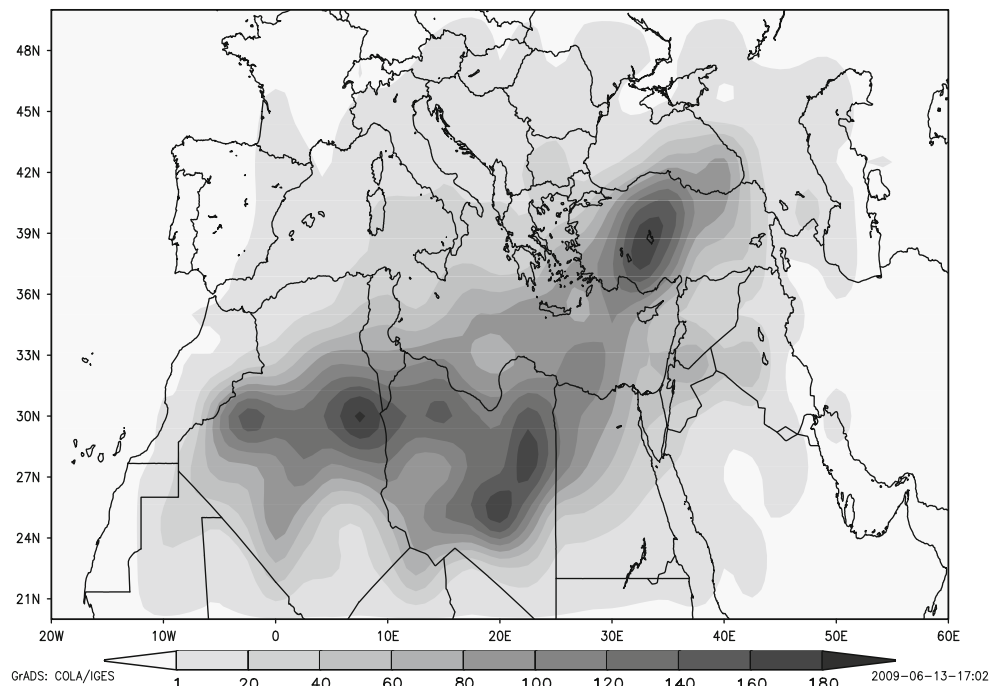


Fig. 6 Density of Saharan cyclones as measured by the number of storms at each grid

over the North Atlantic where the storm track is active and also because of the decreasing zonal distances as we move poleward. When longer tracks are considered the distribution changes and we now get a maximum at 2-day lifespan (Fig. 7). The number of tracks of longevity <2 days travelling long distances (as defined above) has decreased (Fig. 7) because of speed constraints.

3.2 Cyclogenesis and cyclolysis

Cyclone sources and sinks are important to identify because they help understand and quantify the effect of the lower boundary and can be used to validate climate

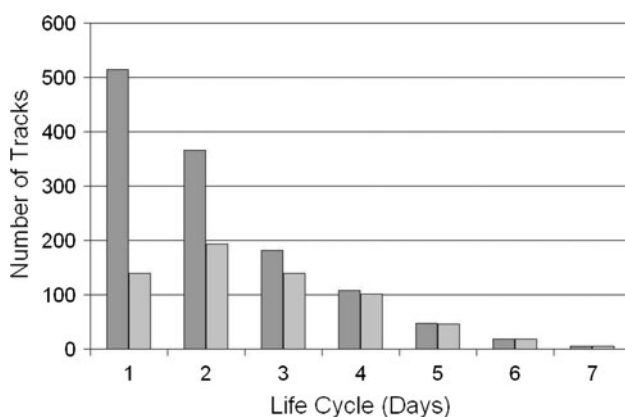


Fig. 7 Number of cyclone tracks defined by longevity for all tracks (dark shading) and tracks spanning more than 20° latitude or 10° longitude (light shading)

models. In an attempt to characterize the sources and sinks of cyclone activity we compute the frequency of tracks initiated in the area (source) and the frequency of tracks in the area where tracks terminate (sinks). The results are shown in Fig. 8, in which cyclogenesis spots can be recognized (Fig. 8, left). First, the lee side of the Atlas chain shows up as the main area of maximum generation of Saharan cyclones, and can be considered as the main source of Saharan cyclones. The Atlas region, in particular, was identified by Trigo et al. (1999)³ as one of the main cyclogenesis centres in the Mediterranean region, which is present more or less throughout the whole year, in particular during the winter (Trigo 2006), and with a peak in May–June. This region is also thought to be a place where enhanced cyclone development over the Apennines and the Adriatic sea originate (Horvath et al. 2006) as well as secondary cyclogenesis following Genoa cyclones (Egger et al. 1995). Next, three other areas located between 21°N and 26°N are identified as secondary sources of Saharan cyclones (Fig. 8, left). The first secondary source region is located south of the Atlas mountains, around 25°N . This cyclogenesis region is identified by Trigo et al. (1999) as a secondary source of cyclone development particularly in May. The second region is located around 15°E and 22°N . The last one is located at about 20°E and 25°N . Another, but weak, source has been identified further south around 5°E . This source region was captured in April by Alpert

³ Recall that the analysis of these authors was based only on a 18-year period of the ECMWF reanalyses.

et al. (1990). These sources are associated with western and central Saharan topography.

The cyclolytic areas are shown in the right panel of Fig. 8 as the number (frequency) of terminated Saharan cyclone tracks. Four main areas of cyclone tracks termination are identified. The primary sink, or main cyclolytic area, is located over central Iraq and north-eastern Arabia. Two secondary sinks are located respectively over mid-west Turkey, centred around 33°E and 39°N, and the western side of the Black Sea, also identified by Trigo (2006) using winter 1,000 hPa height from NCEP/NCAR and ERA-40 reanalyses. The latter centre stretches down to the north of the Fertile Crescent. Another secondary centre is found over the southern tip of Russia, west of the Caspian Sea, around 47°E and 40°N. Apart from these main centres few other marginal areas can be noted over the central Mediterranean, Sardinia and Central Europe (Fig. 8, right).

The sink areas, like the sources, are again determined to a large extent by orography. The previous cyclone track termination areas are associated with the north eastern Arabian mountains and the Anatolian plateau. So in summary, the dominant Saharan cyclone activity in spring tends to move north-eastward, and only a few propagate northward. In addition, most of Saharan cyclones terminate on the Taurus and Zagros mountains, pointing to the importance of orography in cyclolysis. In the lee side of those mountains cyclones are typically regenerated.

Figure 8(right panel) also shows cyclolytic areas over Europe, in particular around Sardinia, the Adriatic Sea and Central Europe. These cyclolytic centres, however, are not as strong as those identified in the eastern flank of the domain due to the fact that the majority of Saharan

cyclones move eastward and only a few of them enter Europe in agreement with results from Hodges (2010, personal communication).

This cyclolytic centre is also present throughout the year, but most prominent in the winter season (Trigo 2006).

4 Cyclone track clustering

4.1 Procedure description

Cyclone tracks are the result of complex nonlinear interacting processes, where local and remote, or teleconnection effects enter into play. For example, Pinto et al. (2009) show that extreme extratropical cyclones tend to occur more frequently during positive NAO phase compared to the negative NAO phase. Hence cyclone tracks are not randomly distributed but follow, on the average, more or less well defined paths or trajectories. These latter result in general from various interacting physical and dynamical processes such as the effect of bottom topography and large scale flow. The objective of this section is to explore the Lagrangian climatology of these tracks by classifying Spring Saharan cyclone tracks using clustering. Clustering of cyclone tracks enables the identification of possible different track regimes. It also enables linkage with the synoptic and large scale atmospheric circulation as well as teleconnection.

In this study we consider the 643 identified tracks for clustering. These tracks span at least 20° latitude and 10° longitude. This choice is made to capture various Saharan cyclones including those travelling north towards Europe. Clustering is known to be a difficult problem. This is

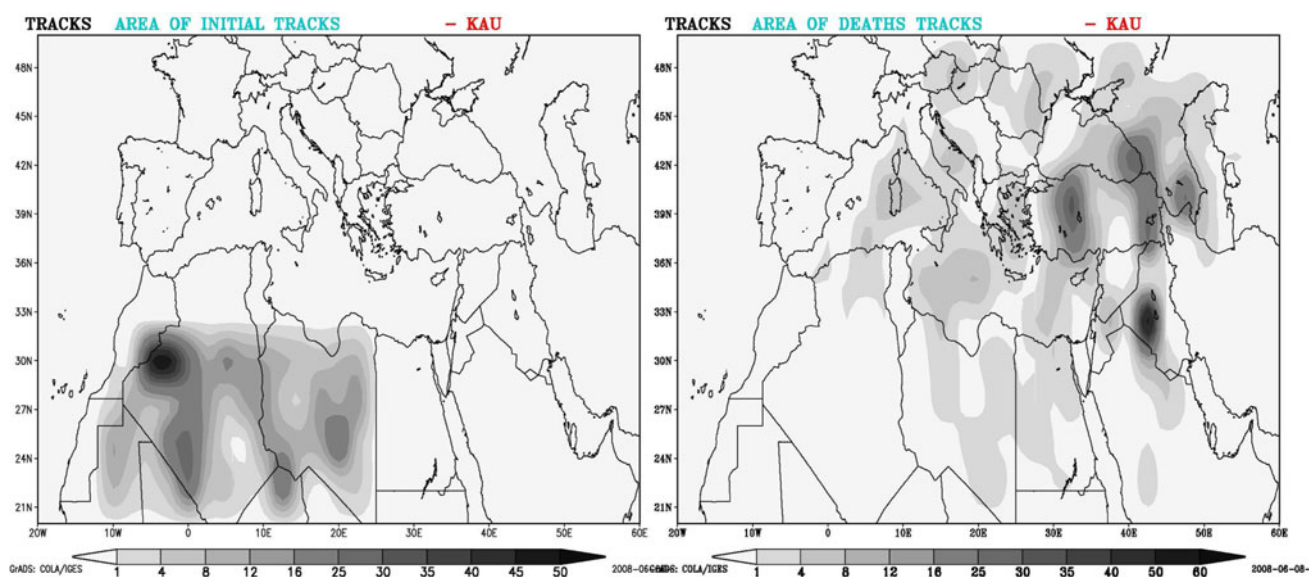


Fig. 8 Number of generated (left) and terminated (right) Saharan cyclones showing respectively areas of Saharan cyclogenesis and cyclolysis

particularly the case when the tracks to be classified have different characteristics. The Saharan cyclone tracks considered here have different lengths and timings. For example, one track may be 2,000 km long and another can be twice as long. In fact, as pointed out by Barry and Chorley (1992) the movement of Mediterranean depressions is highly complex due to both orographic effects and their regeneration over the sea.

In Blender et al. (1997) all cyclones have been subjected to a selection procedure where only those having the same lifetime, fixed to 3 days, were retained. This selection enabled them to map cyclone tracks onto a finite dimensional metric state space where automatic clustering procedures, e.g. k-means, can be applied. Note that k-means does not provide the number of clusters, a much difficult parameter that introduces uncertainty in the clustering method. Note also that while the selection of this parameter may be adequate for the North Atlantic, given the existence of the storm track and the polar jet stream hence the large number of tracks which require an automated procedure in addition to the mapping onto a finite-dimensional metric space, no such indulgence can be afforded here (smaller set with shorter tracks).

Gaffney et al. (2007) used a probabilistic clustering approach to classify wintertime extratropical cyclone tracks over the North Atlantic, whereas Camargo et al. (2007) used the approach to classify tropical cyclone tracks. Their approach is based on a regression mixture model using the Gaussian mixture model (Haines and Hannachi 1995; Smyth and Ghil 1999; Hannachi and O'Neill 2001). The number of clusters, however, remains a difficult problem, see e.g. Hannachi and O'Neill (2001) and Hannachi (2007). Although Gaffney et al. (2007) tried to use “objective” measures to find the number of clusters, based on cross-validation likelihood and predicted sum of squared errors, they recognize that the “objective” measures provided limited guidance in choosing the right number of clusters. It is known, however, that the North Atlantic region is well studied in the tropospheric large scale flow literature, e.g. Kimoto and Ghil (1993), see also Blender et al. (1997). We note here that Gaffney et al. (2007) used three clusters for the North Atlantic cyclone tracks while Camargo et al. (2007) used seven clusters for tropical cyclone tracks.

Classification originates from the field of pattern recognition and constitutes a class of problems that can often be easily solved by human beings, but are very hard to solve by computers (Aart and Korst 1990). Here we use this “human skill” in pattern recognition, given that the objects to be classified can be visualized on the plane. Given that our small set of tracks have different lengths, unlike Blender et al. (1997), we adopt a “subjective” semi-manual method for our track clustering. The tracks have

been first thoroughly examined by eye in an attempt to get a sense of what is going on. Aided with our prior knowledge of the climatology of the region, a maximum of 10 “model” tracks have been initially defined and used to classify the observed tracks. The model tracks are simple curves that stretch between the eastern and western boundaries of the domain, and have various (but simple) shapes and orientations. Each identified track is classified based on its Euclidean (semi-) distance (d) to, and its (semi) spatial correlation (ρ) with, the model tracks. The (semi) distance and correlation are measured between any observed track and the restriction of a model track to the bounding longitudes of the observed track. Our classification procedure is somewhat similar to that of Gaffney et al. (2007) except that our model curves (the equivalent of their regression curves) are chosen “subjectively” in that they are based on visual inspection.

Using the above 10 model curves cyclone tracks are classified based on a minimum correlation of 0.85 and a maximum distance of 450 km. Trigo et al. (1999), for example, consider the typical horizontal scale of Mediterranean cyclones to be 300 km. About 70% of tracks have been classified this way. Next, about 25% of the remaining tracks are classified based on their (semi) distance to the model tracks using a maximum distance of about 750 km. After the clusters are obtained, we examined them visually and found that few clusters are quite similar, and then decided to merge them. This yielded six final clusters, which are discussed next.

4.2 Cyclone track clusters

Six clusters (Fig. 9, Table 1) have been obtained by classifying about 95% of all tracks. These tracks are defined as: (1) Western Atlas–Asia Minor (WAMA), (2) Algerian Sahara–Asia Minor (ASMA), (3) Libyan desert–Asia Minor (LIMA), (4) Algerian Sahara–Egypt (SET), (5) Atlas–Western Europe (AWE), and (6) Algerian Sahara–Central Europe (ACE),

1. Western Atlas–Asia Minor (WAMA); This class (Fig. 9a) is the largest compared to the other clusters and has a sample size of 171 (27%). The tracks of this class are mostly generated in the lee side of the western Atlas chain and the Algerian Sahara. These tracks are oriented north-eastward and cross the northern part of the Libyan Sahara and the eastern Mediterranean to reach Turkey. Some of these tracks extend as far as Ukraine.
2. Algerian Sahara–Asia Minor (ASMA); ASMA tracks (Fig. 9b) are generated in the lee of the western Atlas mountains. Initially zonally oriented, they are almost entirely confined to the Saharan region. They cross Sinai and the north Red Sea to northern Arabia and

- Turkey. This class has 123 tracks, i.e. about 19% of the total number of tracks. They are nearly zonally oriented over Saharan Africa and slightly north-eastward over Turkey, and some of them reach southern Caucasus.
3. Libyan desert–Asia Minor (LIMA); this class (Fig. 9c) is the next largest after WAMA, with 162 tracks (25%). The tracks are generated in the eastern side of the generating area (Fig. 8a), i.e. in the Libyan desert. The tracks extend straight north-eastward over eastern Mediterranean, Turkey and Ukraine.
 4. Algerian Sahara–Egypt (SET); this cluster (Fig. 9d) has a sample size of 46 (7%). The SET tracks are generated in the middle and western part of the initial area. The tracks are mostly confined to the North African desert with a nearly zonal orientation, but most of them do not extend beyond Egypt. Only around 2% of SET tracks stretch to the Middle East. One could argue that WAMA (9a), ASMA (9b) and SET (9d) are similar. However, beside their different orientations and sources these clusters have also different other characteristics such as the distribution of cyclone lifecycles as discussed in the next section.
 5. Atlas–Western Europe (AWE); the tracks of this cluster (Fig. 9e) are generated in the lee side of the western Atlas chain and the western part of the Algerian desert. The tracks then shoot off northward, with a slight eastward shift towards West Europe. The number of tracks in this cluster is 34, i.e. around 5% of the total number of tracks.
 6. Algerian Sahara–central Europe (ACE); the ACE tracks (Fig. 9f) are generated in the middle and the western parts of the initial area, south of the Algerian desert. The tracks extend north-eastward through the Algerian desert and North Libya, then curve northward over the Gulf of Syrt through to central and eastern Europe. This cluster has 74 tracks (12%).

4.3 Track clusters characteristics

The cyclone track clusters differ not only in orientation and lengths but also in lifecycle characteristics. Figure 10 shows, for each cluster, the distribution of the number of storms and mean pressure minimum (in fact pressure minus 980 hPa) over all the tracks versus lifetime bins. As observed previously (Fig. 7), the maximum in all cases is always <4 days. For WAMA (10a), the maximum, about 50%, is obtained with 2 days, and 50% with 1 day. The WAMA cyclones are the fastest moving cyclones given the long distances travelled. Some of these tracks get terminated in the central Mediterranean, south of Sicily, others get terminated in Mid-West Turkey (Fig. 8). Some

cyclones, however, are long lived and survive for up to a week. The ASMA tracks (10b) have a maximum of 35% at 3 days. The cyclones of these tracks are slower than WAMA's presumably because of the weaker westerlies over the Sahara compared to higher latitudes. Some of ASMA cyclones can have up to one week lifespan. LIMA tracks (10c) have comparable frequencies to WAMA's (10a), but with fewer long lived cyclones. SET tracks (10d) have a maximum of nearly 20% at 2 days, but some of the corresponding cyclones can live for up to 6 days. AWE cyclones (10e) take a few days to reach western and central Europe. ACE tracks (10f) have a maximum of about 25% at 3 days, and the associated cyclones can live for up to 6 days.

4.4 Cyclone lifecycles

During their formation cyclones go through growth and decay phases, and it is our intention to investigate, in this section, how and where Saharan cyclones deepen to reach maximum growth. Each track within each cluster is followed by keeping a track record of the pressure values as well as growth rates in addition to the maximum intensity, the minimum pressure and their occurrence times. For this lifecycle compositing each storm is centred on the time at which the minimum pressure occurs. Figure 11 shows the average pressure tendency (solid line) for each cluster. The time origin in Fig. 11 corresponds to the time when cyclone tracks reach their minimum pressure, and it can be seen that maximum growth occurs several hours before pressure minimum occurrence. The shading represents one standard deviation below and above the average. Figure 11 shows similar pressure tendencies around the maximum growth between different clusters with an average of 1.5 hPa/6 h. This value is small compared to extratropical cyclone growth. ASMA (11b) and AWE (11e) have the largest growth (−1.7) followed by SET (−1.6), then ACE, WAMA and LIMA. For all clusters maximum growth occurs about 6 h prior to the lowest pressure. Both the pressure (not shown) and pressure tendency (Fig. 11) show high variability for WAMA, then SET and LIMA. The least variability is obtained with AWE (11e). The deepest cyclones are obtained with WAMA, LIMA, SET and ACE. The WAMA (Fig. 9a) and LIMA (Fig. 9c) tracks cross the central Mediterranean through the Aegean Sea, a region of cyclogenesis activity in the spring and summer seasons. The ACE tracks (9f) travel over a source region located in the north western part of Algeria in April whereas the SET tracks (9d) cross a source region situated in central Libya (Fig. 8). Table 2 shows the distribution of the number of tracks as a function of pressure minima. Pressure minima (not shown) can go down to 985 hPa, obtained with WAMA, and the largest pressure minimum (1,000 hPa) is

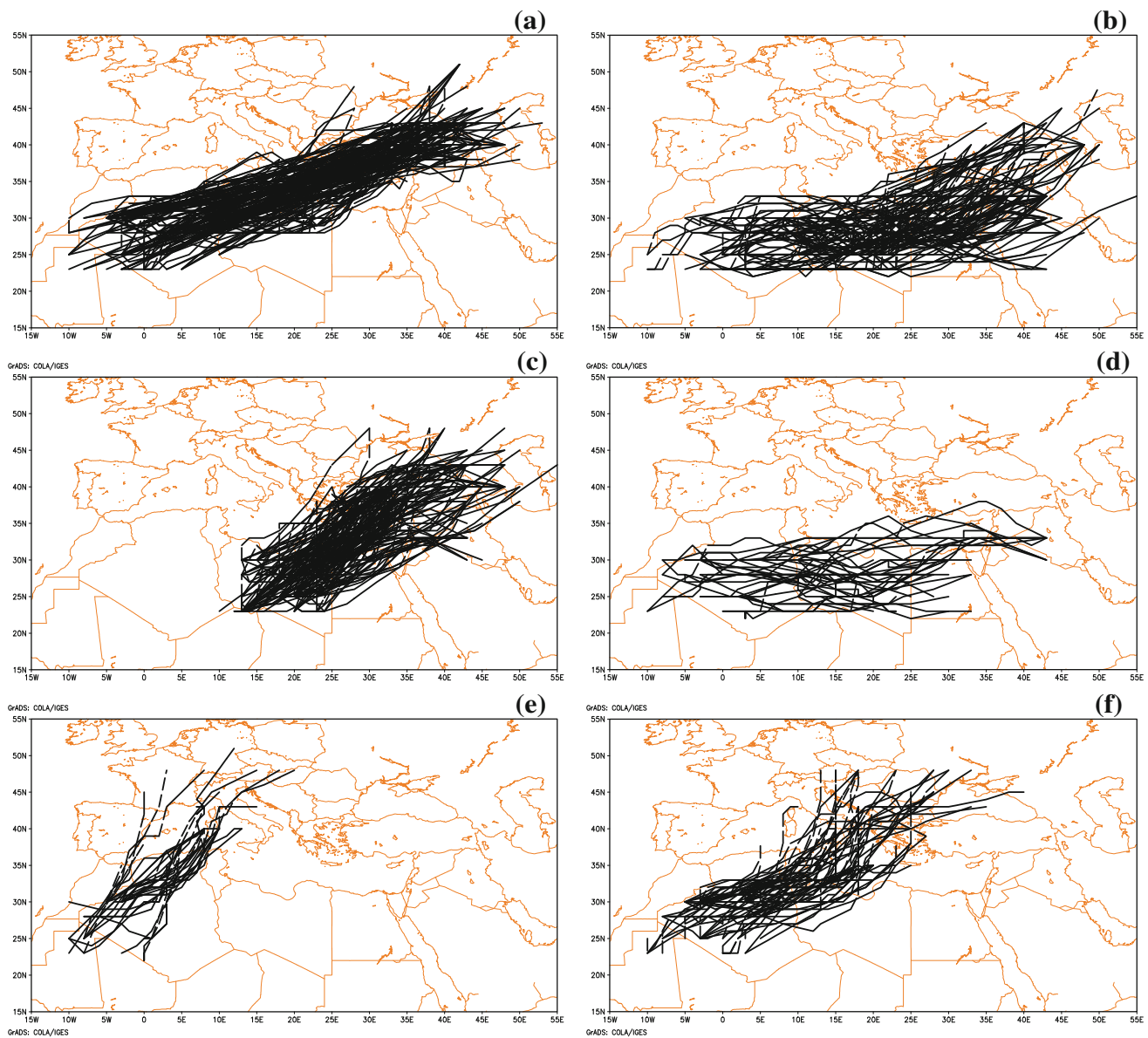


Fig. 9 Identified cyclone track clusters; WAMA (a), ASMA (b), LIMA (c), SET (d), AWE (e) and ACE (f)

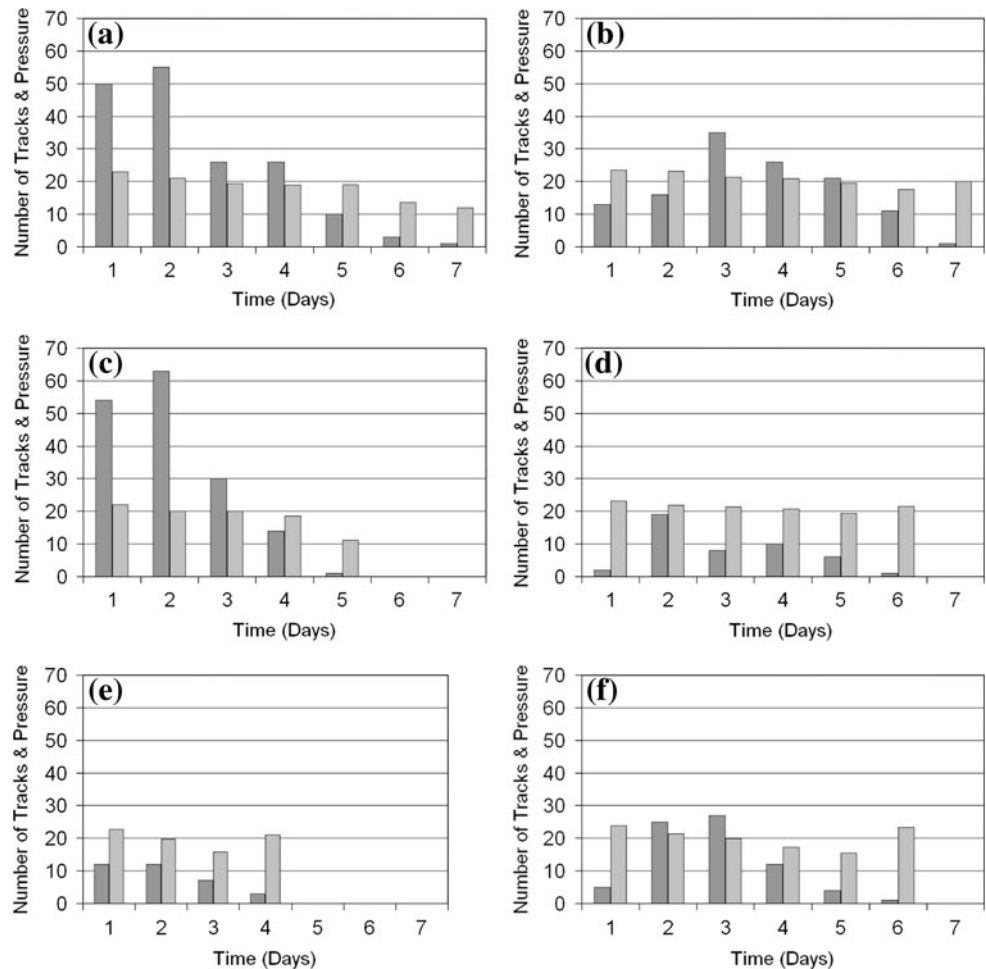
Table 1 Number and percentage of tracks in each cluster

Cluster	WAMA	ASMA	LIMA	SET	AWE	ACE
Number of tracks	171	123	162	46	34	74
%	27	19	25	7	5	12

obtained with ASMA. Figure 11 shows that the time between the beginning of pressure falling and maximum growth (growth time) varies between clusters. This time is largest for WAMA (around 60 h, 11a), and then SET (11d) and LIMA (48 h, 11c). The tracks of these clusters can be classified as long-lived. The growth time for the remaining (short-lived) clusters are of the order of 22 h. The variability of cyclone growth is large for most clusters, and this

reflects one of the main characteristics of Saharan cyclones, in addition to being shallow compared to midlatitude cyclones. Saharan cyclones are short lived compared to midlatitude cyclones (Alpert and Ziv 1989). The time between the beginning of pressure falling and the maximum intensity is of the order of 72 h for midlatitude cyclones (Bengtsson et al. 2009) whereas it is only around 48 h for Saharan cyclones (Fig. 11). Furthermore, Saharan cyclones can reach a minimum pressure of 980 hPa. This is comparatively larger than the North Atlantic low pressure systems, which can go down to 912–915 hPa, see e.g. the recent account of the lowest depressions that crossed the British Isles within the period of instrumental records by Burt (2007). For comparison with models’ simulations

Fig. 10 Number of storms (*dark shading*) and average of pressure minima over all tracks (*light shading*) in particular lifetime bins for WAMA (a), ASMA (b), LIMA (c), SET (d), AWE (e), and ACE (f). The units shown in the vertical axis represent the number of tracks and pressure -980 hPa. For example, the number 10 represents 10 tracks (for *dark shading*) and $980 + 10 = 990$ hPa (for *light shading*)



Bengtsson et al. (2009) obtain 955 hPa for midlatitude cyclones based on ECHAM5 model. Note, however, that in the composites of Bengtsson et al. (2009) the 100 most intense storms were chosen.

Cyclone life cycles are controlled by various factors such as the ambient background flow and boundary conditions. The presence of local permanent (e.g. relief) and semi-permanent (e.g. warm sea surface temperature) features can enhance cyclone growth. Here we have attempted to check this hypothesis by looking at the locations where cyclones reach their maximum growth. Figure 12 shows grid points where the maximum growth occurs. To have a full picture the figure shows both the location of maximum growth in relation to cluster type (12a) and the same locations irrespective of cluster type but with the size of the patches proportional to the number of maximum growth occurrences at each grid point (12b). Different symbols are used for different clusters (Fig. 12a). Few grid points of maximum growth appear separated from their associated tracks. This is because the intensity is based on the original NCEP resolution whereas the tracks are based on interpolation using $1^\circ \times 1^\circ$ latitude–longitude grid. Large patches

in Fig. 12b reflect locations where several cyclones from different clusters reach their maximum intensity. Three broad regions can be identified from the figure where cyclones have tendency to reach their maximum growth. The first one is in the Maghreb, centred over Algeria. The second region is centred over Libya, and the third one is in Turkey and eastern Black Sea. The third location centred over Turkey is the place where a relatively large number of Saharan cyclone tracks reach their maximum intensity. Figure 12 also shows that maximum growth, occurring several hours prior to the lowest pressure, takes place mostly over land and little over the Mediterranean, similar to what has been reported in Alpert and Ziv (1989).

4.5 Synoptic feature

To analyse the climatology of the synoptic situation associated with the identified clusters times of maximum growth are identified for each track in each cluster. Composites of the SLP anomalies are then computed. Figure 13 shows the obtained anomalies for the different clusters. No attempt is made to compute significance levels of the composites

Fig. 11 Pressure tendency versus time for WAMA (a), ASMA (b), LIMA (c), SET (d), AWE (e), and ACE (f). The shading represents one standard deviation below and above the average. Time unit is 6 h with respect to the minimum pressure occurrence, and pressure tendency in hPa/6 h

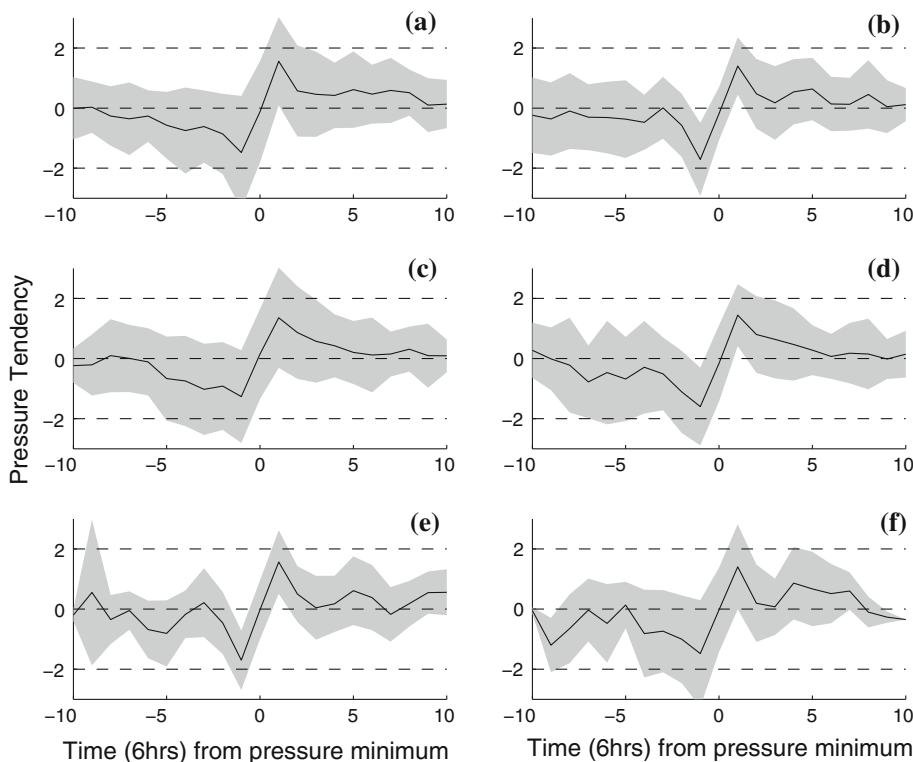


Table 2 Number of tracks, for each cluster, as a function of pressure minimum

Pressure (hPa)	1	2	3	4	5	6
980–985	0	0	1	2	0	0
985–990	2	1	2	0	0	0
990–995	15	5	11	6	0	0
995–1,000	50	32	43	26	14	14
1,000–1,005	81	74	93	32	29	16
1,005–1,010	23	11	12	8	3	4

because of the small sample size of the tracks in the clusters, and we content to discuss the qualitative features of these maps. The pattern associated with the maximum growth for WAMA cyclones (13a) shows two centres; one located over Algeria (−4 hPa) and a deeper one located over Turkey (−5 hPa). Note that these two centres are situated on the main axis of WAMA tracks. The variance of the centre situated over Turkey is more than twice that of the Algerian centre (not shown). In agreement with Fig. 12 some WAMA cyclones deepen over the North African desert while others deepen over Turkey. The climatology of maximum growth flow for ASMA (13b) shows a low over the Libyan desert. This low is the smallest, in magnitude, of all other lows shown in Fig. 13. LIMA maximum growth climatology (13c) shows a major low centre over western Turkey. Maximum growth of LIMA cyclones seems to happen over

Turkey as shown in Fig. 13 although some do happen over Libya (Fig. 12). The main growth centre of SET tracks (13d) is over the Libyan–Algerian desert, see also Fig. 12. The AWE clusters (9e) have the deepest trough (13e) compared to the remaining clusters. The comparison of the orientation of the AWE tracks (9e) and their maximum growth composite (13e) in addition to the depth of the latter, compared to the remaining maps, suggests an influence of the North Atlantic eddy-driven jet stream. This is corroborated by the variance map associated with the composite of Fig. 13e (not shown), which is stronger than the other variance maps, with main local centres located over north western Algeria, Spain and another slightly stronger centre over the North Atlantic west of the Iberian peninsula. Finally, the SLP climatology associated with the maximum growth of ACE tracks (13f) has the next deepest low after AWE. The maximum growth region stretches from southern Tunisia through to Italy around Genoa, southern France and eastern Spain. This region is known for its severe storms in various seasons, particularly in fall (Ouali et al. 2008). Examination of the maximum growth locations of the cyclone tracks in connection with locations of pressure minima and the fact that the Mediterranean sea surface temperature is near its annual minimum in spring suggest that the Genoa low pressure in Fig. 13f reflects the place where some Saharan cyclones reach their maximum intensity. Genoa cyclogenesis is mainly observed in winter as suggested by Alpert and Ziv (1989).

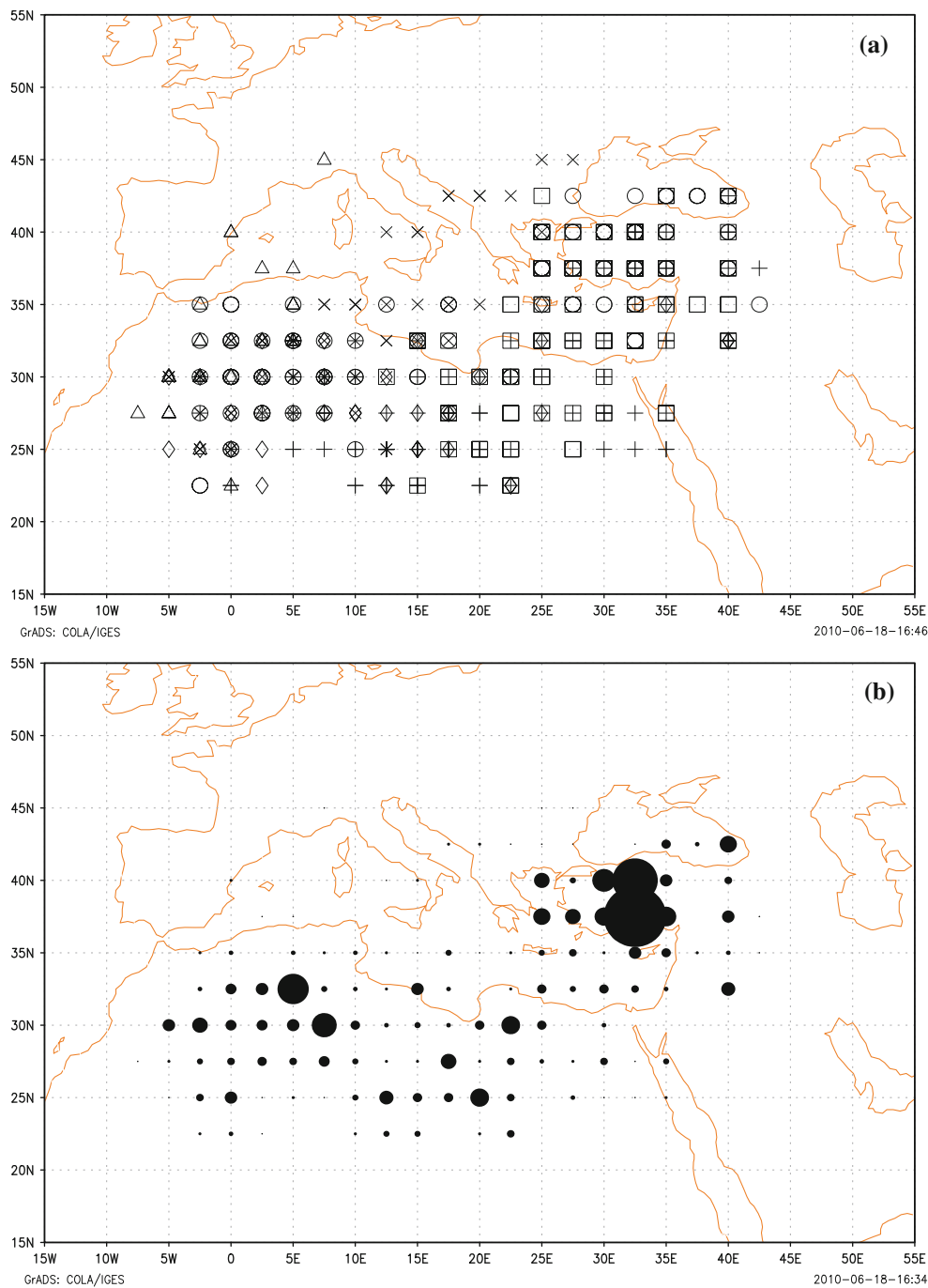


Fig. 12 **a** Location of the maximum intensity for all tracks in all clusters; WAMA (*open circles*), ASMA (*plus symbol*), LIMA (*open square*), SET (*open diamond*), AWE (*open triangle*), and ACE (*multi*

symbol), and **b** same as (**a**) but now the size of the *filled circles* is proportional to the number of events of maximum growth at each grid point

Besides the sea-level pressure composites shown in Fig. 13 we have also computed upper level concurrent composite maps for each of the different clusters in order to infer possible large scale mechanisms involved in the evolution of the Saharan cyclones. The obtained composites, using the 300-hPa geopotential height anomalies, are shown in Fig. 14. The upper level composite maps

(Fig. 14) show similar features to those of the sea level pressure maps (Fig. 13) with a clear vertical westward tilt for virtually all clusters. The strongest upper level anomalies are obtained, in decreasing order, for ACE (−120 m, 14f), AWE (−110 m, 14e), LIMA (−30 m, 14c) and WAMA (−10, 14a). The remaining two clusters have positive height anomaly minima of the order 10–20 m. The

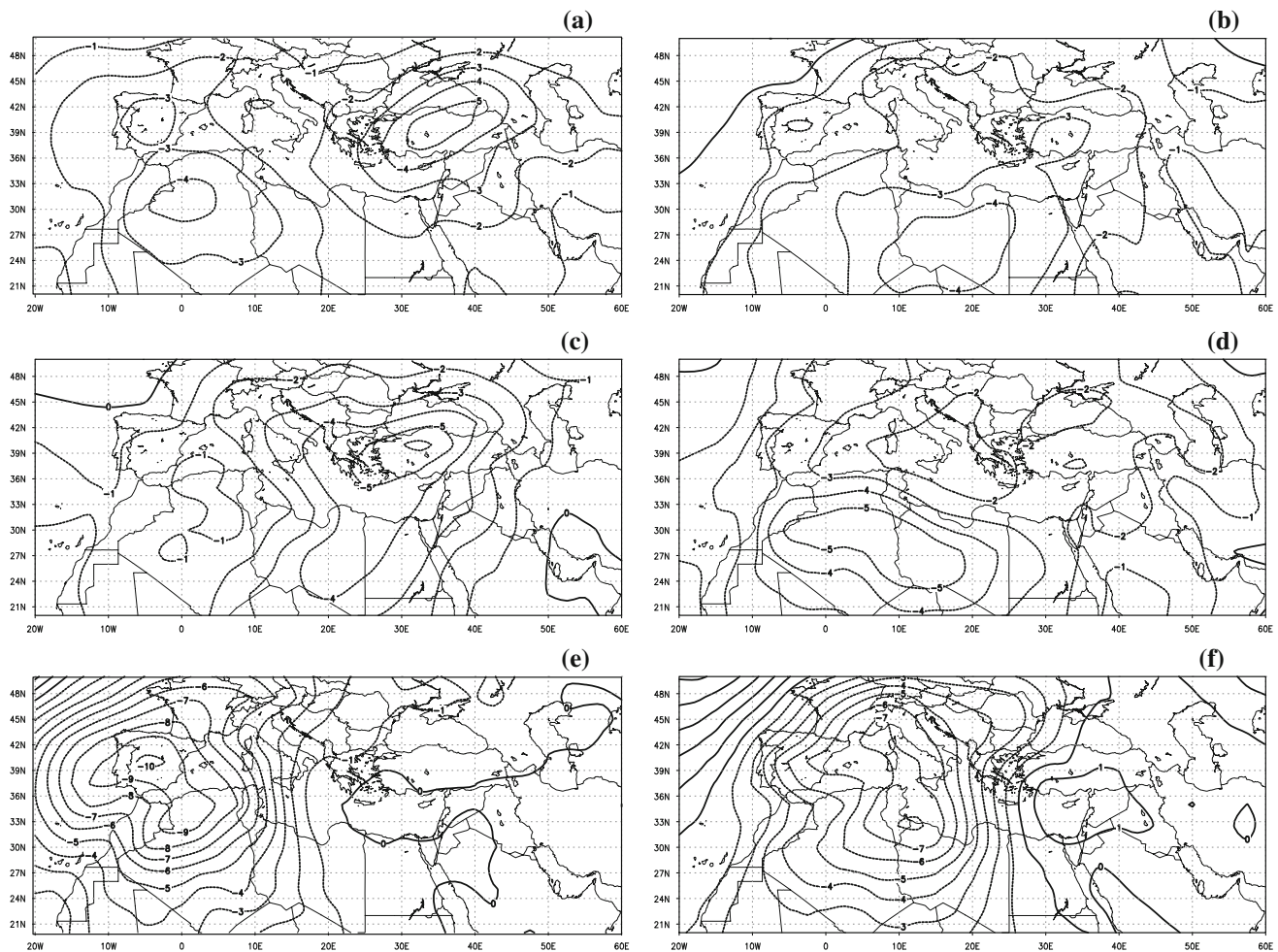


Fig. 13 Composite maps of SLP at maximum growth of cyclone tracks for WAMA (a), ASMA (b), LIMA (c), SET (d), AWE (e), and ACE (f). Contour interval 1 hPa

vertical tilt of the composite maps (Figs. 13, 14) is a clear indication of the role of large scale baroclinicity as pointed out by Alpert and Ziv (1989). In addition, the meridional stretching of the height anomalies with their southwest–northeast tilt is an indication of maximum poleward eddy heat (and momentum) transport (Holton 1992).

5 Summary and discussion

Saharan cyclones in the spring time constitute one dominant feature of the Sahara in the wake of the Siberian High decline towards late winter/early spring (Panagiotopoulos 2005). Permanent features, e.g. topography, and non-permanent features, e.g. large-scale flow and possibly latent heat fluxes⁴ from the Mediterranean sea, enable Saharan

cyclone growth. Given the importance of the Sahara in the climate system and the very limited number of Saharan related studies in the literature, we have conducted a climatological investigation of Spring Saharan cyclone tracks. The main objective here was to document, classify and characterize Saharan cyclone tracks in the spring time. These Spring Saharan cyclones could possibly constitute an initiating mechanism for Saharan dust storms, which peak in February–March–April and are known for their large scale effect including their major influence on the energy distribution of the Earth/atmosphere system and their ability to fertilize the Atlantic phytoplankton (Jickells et al. 2005) and the Amazonian rainforest (Koren et al. 2006).

Six hourly spring (March–April–May) SLP from NCEP/NCAR reanalyses for the period 1958–2006 over the region (10°W–50°E, 20°N–50°N) are used during the spring season. Also, because of the importance of topography in cyclogenesis, the western part of the Sahara, around the Atlas heights, was focussed on to identify cyclogenetic areas. Cyclone centres are first identified within the

⁴ Alpert and Ziv (1989), however, suggest that latent heat may not constitute a major factor in Saharan cyclone maintenance or cyclogenesis.

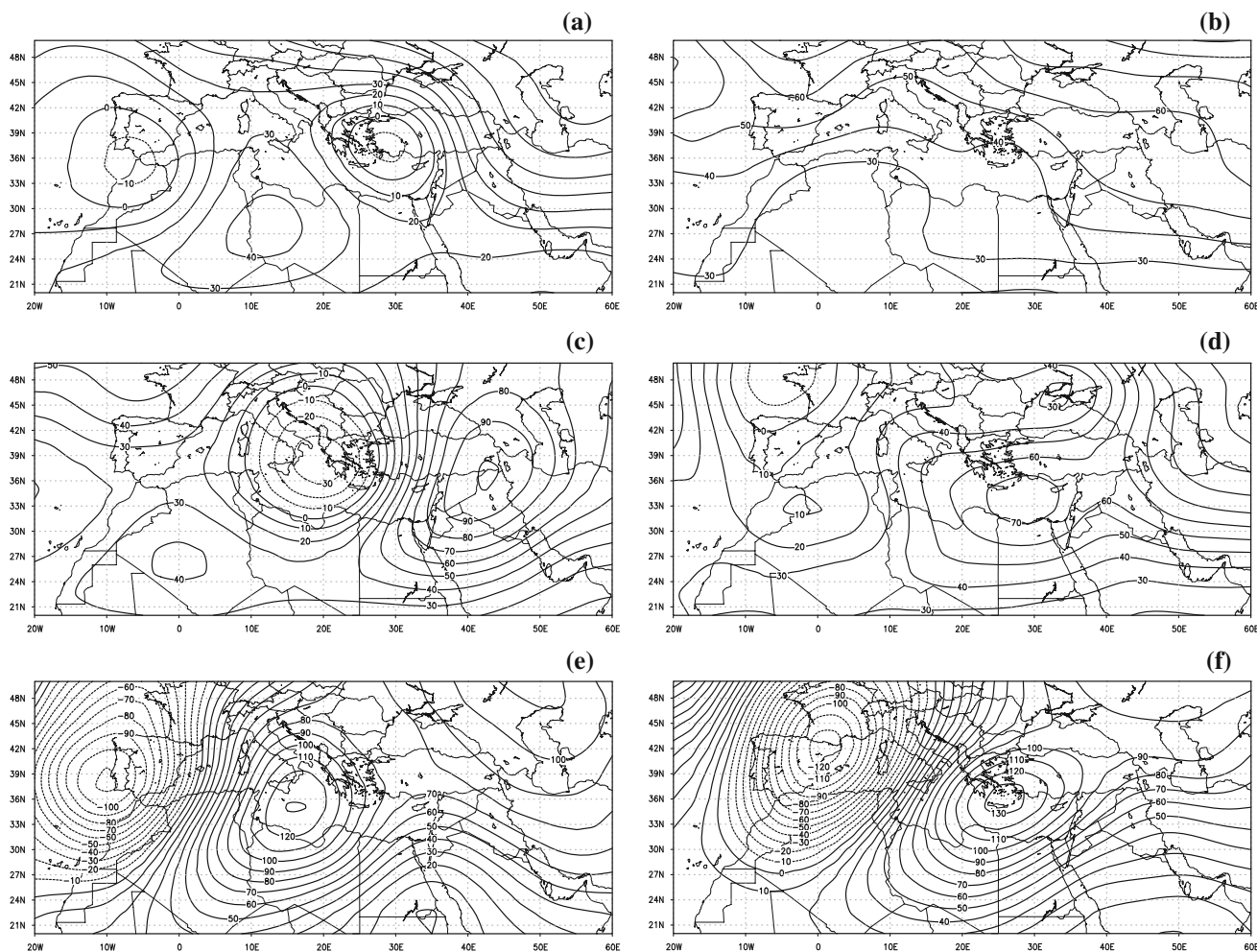


Fig. 14 As in Fig. 13 but for the 300-hPa geopotential height anomalies. Contour interval 10 m

generating area, then cyclone tracks are obtained by following the minimum pressure centres that are less than 1,008 hPa.

A total of 643 tracks have been identified during the considered 49 springs. A large number of these tracks are oriented mostly north-eastward. The frequency of cyclone tracks decreases exponentially with increasing life span, with an e-folding time of about 3 days. Cyclogenetic and cyclolytic areas have been identified. The lee side of the western Atlas chain shows up as the main area of maximum cyclogenesis, which can be considered as the main source of Saharan cyclones, in agreement with previous studies. Three other secondary sources of cyclogenesis are identified over south of the Algerian border, north of Niger/south of Algeria and Libya, and middle of southern Libya. Several centres of cyclolysis have been identified. The main centre is located over central Iraq. Two other centres are identified in mid-west Turkey, and western Black Sea. Another centre is found west of the Caspian Sea.

Next, the identified tracks have been classified. To avoid the complication related to the choice of the number of clusters, a subjective procedure based on visual inspection of the tracks is adopted. Six track clusters have been identified, which are: (1) Western Atlas–Asia Minor (WAMA, 27%); (2) Algerian Sahara–Asia Minor (ASMA 20%); (3) Libyan desert–Asia Minor (LIMA 25%); (4) Algerian Sahara–Egypt (SET 8%); (5) Atlas–western Europe (AWE 8%); and (6) Algerian Sahara–Central Europe (ACE 12%). WAMA and LIMA appear to have a large number of tracks with life time less than about 3 days. ASMA cluster is the one with more long-lived tracks with around 13% of all tracks between 3 and 6 days compared to 9% for WAMA, and 7% for LIMA and ACE. The AWE tracks are shorter lived (4 days maximum) compared to those of the remaining clusters. The average minimum pressure of the track clusters are comparable and there is a tendency for long-lived tracks to be deeper. Cyclone lifecycles for each cluster have been computed.

The maximum growth is obtained with WAMA followed by SET, ACE, LIMA, and is least for AWE. For all cases, the minimum pressure is found to be bounded from below by about 980 hPa compared to about 915 hPa for extratropical cyclones. The highest variability of cyclone life-cycles is observed with WAMA, SET, and LIMA. The expected time between the beginning of pressure falling and maximum growth is around 48 h, compared to 72 h for midlatitudes. In addition, the deepening rate is more or less monotonic, and the maximum growth often occurs 6–8 h prior to pressure minimum, compared to around 30 h for mid-latitude cyclones. These characteristics make clear the distinction between mid-latitude and Saharan cyclones. Regions where pressure minima occur have been identified. We found, in particular, that cyclones have a tendency to reach their maximum growth in three broad regions; the central Maghreb, central Libya, and central Turkey/eastern Black Sea where a large number of Saharan cyclone tracks reach their maximum intensity. Most importantly is the fact that growth occurs mostly over land and little over the Mediterranean in agreement with Alpert and Ziv (1989). The relationship between Saharan cyclone tracks and large scale circulation and teleconnections is another important issue and is left for future research. The composite maps associated with maximum growth show a general agreement between synoptic SLP features and the orientation of the associated tracks. The deepest trough is found with AWE cluster, suggesting a feedback from the North Atlantic eddy-driven jet stream, and the ACE cluster. The strength of these troughs, however, remain smaller compared to their mid-latitude counterparts.

In relation to the Mediterranean basin Trigo et al. (1999), based on a rather short ERA-40 period, found that the Atlas region is the strongest centre for cyclogenesis for Mediterranean cyclones in spring months. This study shows that a substantial amount of Saharan cyclone tracks cross the Mediterranean and one could wonder whether there is a mixing between Saharan and Mediterranean cyclones. One way to distinguish between the two is to examine the location of maximum growth. This study shows that most of these locations are found over the Sahara and a much smaller number over the Mediterranean. According to Alpert and Ziv (1989), in spring time the Mediterranean temperature is near its annual minimum while the continents have reached considerable heating, implying an additional baroclinic source of energy for the Saharan cyclones. Taken together, these facts suggest that the majority of the observed cyclones in this study could be of Saharan origin. A thorough investigation of this issue is, however, beyond the scope of this paper and is left for future investigation. Upper level flow shows agreement with the sea level pressure structure with a clear vertical tilt

pointing to the role of large scale baroclinicity in the growth of Saharan cyclones.

This study is a first contribution to identify the most important cyclones that end up in Arabia and the Middle East in general because these cyclones are an important source of water in the region, and along these lines one of the potentially important future research is to investigate the precipitation characteristics of these Saharan storms. For example, monsoonal-type cyclones reaching Arabia from the Indian Ocean are expected to have different precipitation characteristics compared to cyclones from the Sahara/Mediterranean or the Sudan region. In addition, since the focus region here is where subtropical jet exists the role of this jet in characterising Saharan cyclones will also be addressed in a future research. The link between Spring Saharan cyclones and dust storms is also a subject of great potential interest to climate scientists (Knippertz and Fink 2006). A special issue of *Tellus* was devoted to the SAMUM-1 campaign in southern Morocco in May–June 2006 (e.g., Heintzenberg 2009; Knippertz et al. 2009; Müller et al. 2009), see also Moulin et al. (1997) and Dayan et al. (2007). For example, Knippertz et al. (2009) found that significant dust emission events are connected in part to lee cyclogenesis south of the Atlas mountains. Another equally important issue in the study of Saharan cyclones is the resolution of the gridded data as these cyclones are rather weak compared to cyclones in other regions, e.g. tropics or mid-latitudes. So a potential area for future research is to consider ERA40 or the new Interim reanalyses, at even higher resolution, which can simulate these systems better. In order to increase the chance of capturing more cyclones, spectrally smoothed vorticity may be a better field to use.

Acknowledgments The authors would like to thank two anonymous reviewers for their constructive comments that helped improve the manuscript. Thanks are also due to K. Hodges and J.G. Pinto for their comments on an earlier version of the paper and M. Abdelrahim for his help in preparing Fig. 1.

References

- Aart E, Korst J (1990) Simulated annealing and Boltzmann machine. Wiley, New York
- Agee EM (1991) Trends in cyclone and anticyclone frequency and comparison with periods of warming and cooling over the Northern Hemisphere. *J Clim* 4:263–267
- Alexandersson H, Tuomenvita H, Schmith T, Iden K (2000) Trends of storms in NW Europe derived from an updated pressure dataset. *Clim Res* 14:71–73
- Alpert P, Ziv B (1989) The Sharav cyclone: observations and some theoretical considerations. *J Geophys Res* 94:18495–18514
- Alpert P, Neeman BU, Shay-El Y (1990) Climatological analysis of Mediterranean cyclones using ECMWF data. *Tellus* 42A:65–77

- Andrae U, Sokka N, Onogi K (2004) The radiosonde temperature bias correction used in ERA-40 project. Report series no. 15, Reading, pp 1–34
- Bannon PR (1992) A model of rocky mountain lee cyclogenesis. *J Atmos Sci* 49:1510–1522
- Barry RG, Chorley RJ (1992) Atmosphere, weather and climate, 6th edn. Routledge, London, pp 392
- Bengtsson L, Hodges KI, Keenlyside N (2009) Will extra-tropical storms intensify in a warmer climate. *J Clim* 22:2276–2301
- Blender R, Fraedrich K, Lunkeit F (1997) Identification of cyclone track regimes in North Atlantic. *Q J R Meteorol Soc* 123:727–741
- Burt S (2007) The lowest of the Lows extremes of barometric pressure in the British Isles. Part 1. The deepest depressions. *Weather* 62:4–14
- Camargo SJ, Robertson AW, Gaffney SJ, Smyth P, Ghil M (2007) Cluster analysis of typhoon tracks. Part I: General properties. *J Clim* 20:3635–3653
- Chung Y-S, Hage KD, Reinel ER (1976) On lee cyclogenesis and airflow in the Canadian Rocky mountains and the East Asian mountains. *Mon Wea Rev* 104:879–891
- Dayan U, Ziv B, Shoop T, Enzel Y (2007) Suspended dust over south eastern Mediterranean and its relation to atmospheric circulation. *Int J Climatol* 28:915–924
- Duchon CE (1979) Lanczos filtering in one and two dimensions. *J Appl Meteorol* 18:1016–1022
- Egger J, Alpert P, Tafferner A, Ziv B (1995) Numerical experiments on the genesis of Sharav cyclones: idealised simulations. *Tellus* 47A:162–174
- Elfandy MG (1940) The formation of depressions of the Khamsin type. *Q J R Meteorol Soc* 66:325–335
- Flocas AA (1988) Frontal depression over the Mediterranean sea and Central Southern Europe. *Mediterranée* 4:43–52
- Gaffney SJ, Robertson AW, Smyth P, Camargo SJ, Ghil M (2007) Probabilistic clustering of extratropical cyclones using regression mixture models. *Clim Dyn* 29:423–440
- Guerzoni S, Chester R (1996) The impact of desert dust across the Mediterranean. Kluwer, Dordrecht, pp. 387
- Gulev SK, Zolina O, Grigoriev S (2001) Extratropical cyclone variability in the Northern hemisphere winter from the NCEP/NCAR reanalysis data. *Clim Dyn* 17:795–809
- Haak U, Ulbrich U (1996) Verification of an objective cyclone climatology for the North Atlantic. *Meteorol Zeits* 5:24–30
- Haines K, Hannachi A (1995) Weather regimes in the Pacific from a GCM. *J Atmos Sci* 52:1334–1348
- Hannachi A (2007) Tropospheric planetary wave dynamics and mixture modeling: two preferred regimes and a regime shift. *J Atmos Sci* 64:3521–3541
- Hannachi A, O'Neill A (2001) Atmospheric multiple equilibria and non-Gaussian behaviour in model simulations. *Q J Roy Meteorol Soc* 127:939–958
- Hanson CE, Palutikof JP, Davies TD (2004) Objective cyclone climatologies of the North Atlantic—a comparison between the ECMWF and NCEP reanalyses. *Clim Dyn* 22:757–769
- Hayden BP (1981) Secular variation in Atlantic Coast extratropical cyclones. *Mon Wea Rev* 109:159–167
- Heintzenberg J (2009) The SAMUM-1 experiment over Southern Morocco: overview and introduction. *Tellus* 61B:2–11
- HMSO (1962) Weather in the Mediterranean. I. General meteorology, second edn. Her Majesty's Stationery Office, pp. 362
- Hodges KI (1995) A general method for tracking analysis and its application to meteorological data. *Mon Wea Rev* 122:2573–2586
- Holton JR (1992) An introduction to dynamic meteorology, third edn. Academic Press, San Diego
- Hodges KI, Hoskins BJ, Boyle J, Thorncroft C (2003) A comparison of recent reanalysis using objective feature tracking: storm tracks and easterly waves. *Mon Wea Rev* 131:2012–2037
- Horvath K, Fita L, Romero R, Ivancan-Picek B, Sriperski I (2006) Cyclogenesis in the lee of the Atlas mountains: a factor separation numerical study. *Adv Geosci* 7:327–331
- Hoskins BJ, Hodges KI (2002) New perspectives on the Northern Hemisphere winter storm tracks. *J Atmos Sci* 59:1041–1061
- Jickells TD, An Z S, Andersen KK, Baker AR, Bergametti G et al (2005) Global iron connections between desert dust, ocean biochemistry, and climate. *Science* 308:67–71
- Kalnay E, Kanamitsu M, Kistler R, Collins W, Deaven D, Gandin L, Iridell M, Saha S, White G, Woollen J, Zhu Y, Chelliah M, Ebisuzaki W, Higgins W, Janowiak J, Mo KC, Ropolewski C, Wang J, Leetma A, Reynolds R, Jenne R, Joseph D (1996) The NCEP/NCAR 40-year reanalysis project. *Bull Am Meteorol Soc* 77:437–471
- Kimoto M, Ghil M (1993) Multiple flow regimes in the northern hemisphere winter. Part II. Sectorial regimes and preferred transitions. *J Atmos Sci* 16:2645–2673
- Kistler R, Collins W, Saha S, White G, Woollen J, Kalnay E, Chelliah M, Ebisuzaki W, Kanamitsu M, Kousky V, van den Dool H, Jenne R, Fiorino M (2001) The NCEP/NCAR 50-year Reanalyses: monthly CD-ROM and documentation. *Bull Am Meteorol Soc* 82:247–267
- Klein WH (1957) Principal tracks and mean frequencies of cyclones and anticyclones in the Northern hemisphere. Research paper 40, U.S. Weather Bureau, pp 1–60
- Knippertz P, Fink AH (2006) Synoptic and dynamic aspects of an extreme springtime Saharan dust outbreak. *Q J R Meteorol Soc* 132:1153–1177
- Knippertz P et al (2009) Dust mobilization and transport in the northern Sahar during SAMUM 2006—a meteorological overview. *Tellus* 61B:12–13
- Koren I, Kaufman Y J, Washington R, Todd MC, Rudich Y et al (2006) The Bodélé depression: a single spot in the Sahara that provides most of the mineral dust to the Amazonas forest. *Environ Res Lett* 1:1–5
- Lin, Y-L, Chen S-Y, Hill CM, Huang C-Y (2005) Control parameters for the influence of a mesoscale mountain range on cyclone track continuity and deflection. *J Atmos Sci* 62:1849–1866
- Moulin C, Lambert CE, Dulac F, Dayan U (1997) Control of atmospheric export of dust from North Africa by the North Atlantic Oscillation. *Nature* 387:691–694
- Müller D et al (2009) EARLINET observations of the 14–22-May long-range dust transport event during SAMUM 2006: validation of results from dust transport modelling. *Tellus* 61B:325–339
- Murray RJ, Simmonds I (1991) A numerical scheme for tracking cyclone centres from digital data. Part I. Development of and operation of the scheme. *Aust Meteorol Mag* 39:155–166
- Ouali A, Chaabane M, Maalej A, Hannachi A, Fucello A (2008) The Tunisian storm of 16–18 September 2003: a diagnostic study of the synoptic situation. *Weather* 63:122–127
- Panagiotopoulos F (2005) Trends and teleconnections of the Siberian High. PhD Thesis, Departments of Geography and Meteorology, the University of Reading, pp. 170
- Pedgley DE (1972) Desert depressions over north-east Africa. *Meteorol Mag* 101:228–243
- Petterssen S (1956) Weather analysis and forecasting, vol 1: motion and motion systems. McGraw-Hill, New York
- Pinto JG, Spanghe T, Ulbrich U, Speth P (2005) Sensitivities of a cyclone detection and tracking algorithm: individual tracks and climatology. *Meteorologische Zeitschrift* 14:823–838
- Pinto JG, Zacharias S, Fink AH, Leckeboush GC, Ulbrich U (2009) Factors contributing to the development of extreme North

- Atlantic cyclones and their relationship with the NAO. *Clim Dyn* 32:711–737
- Prospero JM, Ginoux P, Torres O, Nicholson SE, Gill TE (2002) Environmental characterization of global sources of atmospheric soil dust identified with Nimbus 7 total ozone mapping spectrometer (TOMS) absorbing aerosol product. *Rev Geophys* 40:1002. doi:[10.1029/2000GR000095](https://doi.org/10.1029/2000GR000095)
- Radinovic D (1987) Mediterranean cyclones and their influence on the weather and climate. PSMP report series 24, WMO, Geneva, pp. 131
- Raible CC, Della-Marta PM, Schwierz C, Wernli W, Blender R (2008) Northern Hemisphere extratropical cyclones: a comparison of detection and tracking methods and different realyses. *Mon Wea Rev* 136:880–897
- Rodwell M, Hoskins BJ (1996) Monsoons and the dynamics of deserts. *Q J Roy Meteorol Soc* 122:1385–1404
- Schinke H (1993) On the occurrence of deep cyclones over Europe and the North Atlantic for the period 1930–1991. *Beitr Phys Atmo* 66:223–237
- Sickmoller M, Blender R, Fraedrich K (2000) Observed winter cyclone tracks in the northern hemisphere in re-analysed ECMWF data. *Q J R Meteorol Soc* 126:591–620
- Simmonds I, Murray RJ, Leighton RM (1999) A refinement of cyclone tracking methods with data from FROST. *Aust Met Mag* (Special Edition), 35–49
- Tantawy AHI (1969) On the cyclogenesis and structure of Spring Sahara depressions in subtropical Africa. *Meteorol Res Bull* (Published by the Dept of Metrol, Cairo, Egypt) 69:68–107
- Thorncroft CD, Flocas HA (1997) A case study of Saharan cyclogenesis. *Mon Wea Rev* 125:1147–1165
- Trigo IF (2006) Climatology and interannual variability of storm-tracks in the Euro-Atlantic sector: a comparison between ERA-40 and NCEP/NCAR reanalyses. *Clim Dyn* 26:127–143
- Trigo IF, Davies TD, Bigg GR (1999) Objective climatology of cyclones in the Mediterranean region. *J Clim* 12:1685–1696
- Trigo IF, Bigg GR, Davies TD (2002) Climatology of cyclogenesis mechanisms in the Mediterranean. *Mon Wea Rev* 117:154–176
- Ulbrich U, Leckebusch GC, Pinto JG (2009) Extra-tropical cyclones in the present and future climate: a review. *Theor Appl Climatol* 96:117–131
- WASA Group (1998) Changing waves and storms in the north-east Atlantic? *Bull Am Meteorol Soc* 79:741–760
- Washington R, Todd MC, Middleton NJ, Goudie ES (2003) Dust-storm source areas determined by the total ozone monitoring spectrometer and surface observations. *Ann Assoc Am Geogr* 93:297–313
- Wernli H, Schwierz C (2006) Surface cyclones in the ERA-40 data set (1958–2001). Part I. Novel identification method and global climatology. *J Atmos Sci* 63:2486–2507